Journal Article

Optimized composition, structure, and property of a low-carbon bio-rejuvenator for aged asphalt

Zhou, X., Zong, T., Yang, C., Kim, S., Li, L., Chen, M., Ma, Z.

Optimized composition, structure, and property of a low-carbon bio-rejuvenator for aged asphalt

Xinxing Zhou[1,2,*], Professor, Ph.D.,

1. Institute of Resources and Environmental Engineering, Shanxi University, Taiyuan 030031, China

2. School of Environmental Science and Engineering, Tianjin University, Tianjin 300350, China

Email: zxx09432338@sxu.edu.cn

Tianqi Zong[1], Ph.D., Candidate

1. Institute of Resources and Environmental Engineering, Shanxi University, Taiyuan 030031, China

Email: zongtianqi1@sxu.edu.cn

Chunping Yang[3], Professor, Ph.D.,

3.College of Environmental Science and Engineering, Hainan University, Haikou, Hainan 570228, China

Email: yangc@hnu.edu.cn

Seung-Soo Kim[4], Professor, Ph.D.,

4.Department of Chemical Engineering, College of Engineering, Kangwon National University, Samcheok-Si 25913, Republic of Korea

Email: sskim2008@kangwon.ac.kr

Linglin Li[5], Senior Lecturer, Ph.D.,

5.Built Environment, Wrexham University, Mold Road, Wrexham LL11 2AW, Wales, UK

Email: linglin.li@wrexham.ac.uk

Meizhu Chen[6], Professor, Ph.D.,

6.School of Materials Science and Engineering, Wuhan University of Technology, Wuhan, 430070, China

Email:chenmzh@whut.edu.cn

Zhibin Ma[1,], Professor, Ph.D.,**

1.Institute of Resources and Environmental Engineering, Shanxi University, Taiyuan 030031, China

Email:mazhibin@sxu.edu.cn

*Corresponding author:

*Xinxing Zhou, Email:zxx09432338@sxu.edu.cn

Present address: Zhanming North Building Room B313, No.63 South central east street, Xiaodian district, Taiyuan, Shanxi Province, China

Tel:+86 13513645248

**Zhibin Ma, Email:mazhibin@sxu.edu.cn

Present address: Zhanming North Building Room B214, No.63 South central east street, Xiaodian district, Taiyuan, Shanxi Province, China

Abstract: Catalytic liquefaction of waste wood and waste tire rubber was conducted to produce bio-oil under varying experimental conditions, including liquefaction temperature, retention time, solvent type, and catalyst type. Subsequently, a bio-oil-activated waste tire rubber **rejuvenator**, referred to as a **bio-rejuvenator** (BRR), was synthesized by adjusting the bio-oil content and optimizing microwave treatment parameters. The microwave activation and structure-property regulation mechanisms of BRR were elucidated. The results indicated that the highest bio-oil yield and aromatic content were achieved under the following conditions: a waste wood-to-waste tire rubber ratio of 6:4, a liquefaction temperature of 200 °C, a residence time of 0.5 h, dichloromethane as the solvent, and Al_2O_3 as the catalyst. Liquefaction temperature had the most significant effect on the structure and properties of bio-oil, followed by solvent and catalyst type, and finally residence time. The flash point, aromatics content, and saturates content of BRR are 375-462 °C, 20.1-21.8%, and 16.4-17.9%, respectively, which meet the road application standards. BRR containing 15-35% bio-oil met the performance requirements for a **rejuvenator.** The microwave activation mechanism revealed that microwaves can break the S-S and C-S bonds in waste tire rubber, increasing molecular flexibility. The -OH and C=O groups in bio-oil can then react with the broken S-S or C-S bonds, forming BRR. The structure-property regulation mechanism of BRR indicates that waste wood contributes to higher aromatic and oxygen content, whereas waste tire rubber increases carbon content and reduces oxygen content. Bio-oil acts as a source of aromatics and saturates, helping to compatibilize the waste tire rubber, soften it, and

reduce the viscosity of BRR.

Keywords: **Bio-rejuvenator**; Composition optimization; Structure-property regulation mechanism; Waste wood; Waste tire rubber

1. Introduction

According to statistics, by the end of 2024, China's expressway network had reached a total length of 190,700 km, with approximately 12% of the network requiring annual maintenance[1-2]. The annual generation of reclaimed asphalt pavement (RAP) is estimated at 20 million tons[3]. After recycling, this process can reduce material costs by up to 31.8 billion yuan[4]. To promote resource conservation and efficient utilization, the Chinese government has implemented policies to encourage the recycling and reuse of waste materials, driving a shift in the transportation sector from prioritizing speed and scale to focusing on quality and efficiency[5-7]. By implementing rational strategies, such as recycling RAP using a **bio-rejuvenator,** significant savings in raw material costs can be achieved[8-9]. This effectively minimizes material waste and environmental pollution[10], positioning RAP recycling as a cornerstone of sustainable infrastructure development. Extensive research has been conducted on the recycling of aged asphalt, with proposed mechanisms broadly categorized into two types: the component compensation mechanism and the reactive regeneration mechanism[11-12].

By the end of 2024, China's stockpile of end-of-life tires had reached approximately 800 million units, with annual waste tire rubber processing capacity exceeding 1 million tons[13-15]. The open burning of discarded tires generates

substantial environmental pollution, releasing hazardous compounds such as polycyclic aromatic hydrocarbons (PAHs) and dioxins[16]. To valorize this waste stream, co-pyrolysis of waste tire rubber with waste wood, particularly enzymatic hydrolysis waste wood, has been investigated to produce bio-oil, with studies focusing on the synergistic interactions between the two feedstocks[17-19]. The distributed activation energy model (DAEM) has been employed to assess the resource recovery potential of end-of-life tire samples during pyrolysis. Notably, the contents of natural rubber, synthetic rubber, and limonene in the resulting pyrolysis oils exhibit strong linear correlations[20]. However, tire-derived pyrolysis oil suffers from inherent drawbacks, including high viscosity and low hydrogen content, which limit its direct use as a fuel or chemical feedstock[21-22].

In recent years, pyrolysis bio-oil derived from waste wood has been extensively investigated as a renewable energy source[23-26]. A novel method for quantifying exothermicity during the pyrolysis of large wood particles, based on interpolated temperature curves, has also been proposed[27]. Furthermore, Al_2O_3-based acid leaching residue has been explored as a catalyst for waste wood pyrolysis, with studies revealing that chlorination of the catalyst surface activates Brønsted acid sites, thereby enhancing furfural selectivity[28]. However, pyrolysis bio-oil is typically characterized by low heating value, high oxygen content, and poor thermal stability[29-34]. Co-pyrolysis of waste wood and waste tire rubber offers a promising strategy to address these limitations. In this approach, both feedstocks are first comminuted and then subjected to co-liquefaction to produce a upgraded bio-oil.

Subsequently, the waste tire rubber component is activated by the bio-oil, and the resulting blend is formulated into a bio-rubber rejuvenator (BRR). This is a new application of bio-oil.

As for aged asphalt rejuvenator, they are mainly two kinds: component-supplementing rejuvenator and reactive rejuvenator[11]. Component-supplementing rejuvenators (e.g., bio-oils, aromatic oils, or softening agents) work by replenishing lost light fractions and improving flexibility. Their advantages include simplicity, low cost, and good compatibility with base materials[11]. However, they may cause excessive softening, poor long-term stability, and limited restoration of original chemical structure. Reactive rejuvenators (e.g., compounds with epoxide, amine, or silane groups) chemically interact with the aged polymer network, breaking cross-links or forming new bonds, to partially restore molecular integrity. They offer better durability and performance recovery but are often more expensive, complex to formulate, and may require precise processing conditions[12]. In summary, component- supplementing types are economical and easy to use but less durable, while reactive types provide superior structural recovery at higher cost and complexity.

This BRR not only restores the elasticity of aged asphalt mixtures but also enhances their toughness, fatigue resistance, and long-term durability[35-37] , demonstrating significant potential for sustainable pavement applications[38-39]. Nevertheless, the optimized composition, structure, and property of a low-carbon BRR for aged asphalt remain unclear, which has hindered its broader application.

To address the aforementioned limitations of BRR, a waste wood- and waste tire rubber-derived bio-oil-activated rubber-referred to as a BRR-was developed through co-liquefaction followed by microwave activation. Furthermore, the optimized composition, structure, and property of a low-carbon BRR for aged asphalt were investigated using a multi-technique approach, including: molecular simulations, Fourier infrared spectrometer (FT-IR), gas chromatography-mass spectrometry (GC-MS), gel permeation chromatography (GPC), Fourier Transform Infrared Microscope (FT-IRM), dynamic shear rheometer (DSR), fluorescence microscopic (FM), and X-ray photoelectron spectrometer (XPS).

2. Materials and experiments

2.1 Raw materials

The raw materials consist of waste wood and waste tire rubber. The waste wood is sourced from pine, while the waste tire rubber is derived from the top components of discarded radial tires. The average particle size of the waste tire rubber is 425 μm and the natural rubber content ranges from 15% to 20%. Proximate analysis data for both materials is presented in **Table 1**. As shown in the table, the volatile matter and ash content of the waste wood together account for over 90% of its total mass. In contrast, waste tire rubber exhibits high levels of volatile matter and fixed carbon, which together constitute more than 90% of its total mass.

Table 1. The proximate analysis of waste wood and waste tire rubber

Type	Ash content	Volatiles	Moisture	Fixed carbon
Waste wood	37.98	52.81	2.29	6.92
Waste tire rubber	9.06	62.14	0.80	28.00

2.2 The preparation of bio-oil

Waste wood and waste tire rubber were mixed in varying mass ratios (9:1, 8:2, 7:3, 6:4, 5:5) and loaded into a hydrothermal reactor for co-liquefaction. Prior to co-liquefaction, waste tire rubber was subjected to **microwave** pyrolysis at 350 °C for 2 h under nitrogen to partially cleave S-S cross-links. The reaction temperature was varied from 180 °C to 280 °C in 20 °C increments, and the residence time ranged from 0.5 to 3 h in 0.5 h increments. The solvents tested included distilled water, dichloromethane, and ethanol, and the catalysts employed were Al_2O_3, CeO_2, MOF, and C/Pt. The experimental preparation parameters are summarized in **Table 2**.

Table 2. The preparation parameters of bio-oil

Sample	Wood/rubber ratio	Temperature (°C)	Time (h)	Solvent	Catalyst	Yield (%)
S1	9:1	180	0.5	water	Al_2O_3	19.1
S2	8:2	180	0.5	water	Al_2O_3	19.5
S3	7:3	180	0.5	water	Al_2O_3	20.1
S4	6:4	180	0.5	water	Al_2O_3	20.5
S5	5:5	180	0.5	water	Al_2O_3	19.2
S6	6:4	200	0.5	water	Al_2O_3	21.2
S7	6:4	220	0.5	water	Al_2O_3	22.7
S8	6:4	240	0.5	water	Al_2O_3	24.5
S9	6:4	260	0.5	water	Al_2O_3	27.3
S10	6:4	280	0.5	water	Al_2O_3	27.5
S11	6:4	200	1	water	Al_2O_3	22.0
S12	6:4	200	1.5	water	Al_2O_3	23.5
S13	6:4	200	2	water	Al_2O_3	25.2
S14	6:4	200	2.5	water	Al_2O_3	25.9
S15	6:4	200	3	water	Al_2O_3	26.2
S16	6:4	200	0.5	dichloromethane	Al_2O_3	31.2
S17	6:4	200	0.5	ethyl alcohol	Al_2O_3	26.5
S18	6:4	200	0.5	water	CeO_2	21.3
S19	6:4	200	0.5	water	MOF	21.8
S20	6:4	200	0.5	water	C/Pt	21.5

As shown in the table, temperature, solvent, and catalyst significantly affect the bio-oil yield, whereas the wood/rubber ratio and residence time have only a slight

influence. The highest bio-oil yield and aromatic content were achieved under the following conditions: a waste wood-to-waste tire rubber ratio of 6:4, a liquefaction temperature of 200 °C, a residence time of 0.5 h, dichloromethane as the solvent, and Al_2O_3 as the catalyst. Thus, when bio-oil yield is used as the optimization criterion, these conditions represent the optimal preparation parameters for bio-oil production.

2.3 The preparation of BRR

Bio-oil was prepared under the optimal conditions identified in Section 2.2. It was then blended with waste tire rubber at mass fractions of 15-35%, and the mixture was subjected to microwave treatment to produce bio-oil-activated rubber. Subsequently, the BRR was formulated by incorporating 20% of this activated rubber into fresh bio-oil. The preparation parameters for BRR are summarized in **Table 3.** Microwave activation was performed in a microwave heating system at power levels of 1000-2000 W for durations of 60-240 s.

Table 3. The preparation parameters of BRR

Number	Bio-oil content (%)	Microwave power (W)	Microwave time (s)
S21	15	1000	60
S22	20	1000	60
S23	25	1000	60
S24	30	1000	60
S25	35	1000	60
S26	30	1500	60
S27	30	2000	60
S28	30	1000	120
S29	30	1000	180
S30	30	1000	240

2.4 The functional groups of BRR

The functional groups of the raw materials (waste tire rubber, bio-oil,

bio-oil-activated rubber, and BRR) were analyzed using Fourier-transform infrared spectroscopy (FT-IR). Additionally, the changes in functional groups of waste tire rubber were examined before and after microwave activation. Spectra were recorded over a wavenumber range of 400-4000 cm^{-1} with a resolution of 2 cm^{-1} and 32 scans per measurement, using attenuated total reflection (ATR) as the sampling mode.

2.5 The chemical structure and composition of BRR

Twenty milliliters (20 mL) of the BRR solution were added to 40mL of dichloromethane. The mixture was vigorously agitated for 1h, then concentrated to approximately 2 mL using a rotary evaporator, followed by nitrogen purging. The chemical composition and structural features of the BRR were characterized via gas chromatography-mass spectrometry (GC-MS).

The chemical composition and sulfur valence state of the BRR were characterized using gas chromatography-mass spectrometry (GC-MS) and X-ray photoelectron spectroscopy (XPS). GC-MS analysis was conducted with an injector at 290 °C, a temperature program from 40 °C (2 min hold) to 290 °C at 4 °C/min (20 min final hold), helium carrier gas (1.2 mL/min), and MS in EI mode (70 eV, ion source 260 °C, transfer line 280 °C, m/z 50-650, 100 ms/scan). For XPS, samples were sputter-cleaned for 30 min using a 3 keV Ar^+ beam, and both survey (0-1100 eV) and high-resolution (C 1s, O 1s, N 1s) spectra were collected in FAT mode without charge neutralization, employing a 200 μm X-ray beam (-50 W), 224 eV pass energy, 0.4 eV step size, 200 ms dwell time, 1 sweep, and 2 cycles.

2.6 The rheological properties of BRR

The rheological properties of the BRR were characterized using a dynamic shear rheometer (DSR). Specifically:

- High-temperature rheological behavior was evaluated with a 25 mm parallel-plate rotor system across the temperature range of 30 °C to 80 °C.
- Low-temperature rheological behavior was assessed using an 8 mm parallel-plate rotor system from -30 °C to 10 °C.

Additionally, the viscosity-temperature dependency of the BRR was investigated using a Brookfield Rotational Viscometer, with temperature sweeping from 60 °C to 200 °C.

2.7 The microstructure of BRR

The microstructure of BRR was evaluated by fluorescence microscope and atomic force microscopy. The magnification times of fluorescence microscope (Shangguang XP63) selected 50X. The samples of fluorescence microscope were heated to liquid and spread flat on the slide as a film with a thickness of 3 to 5 μm.

2.8 Molecular modeling

Bio-oil was represented by the molecular formula $C_7H_8O_2$, as reported in our previous study [40], while rubber was modeled using C_8H_8, based on prior research [19]. The molecular structures of bio-oil and rubber were downloaded from ChemicalBook in MOL file format. The BRR model comprised 27 bio-oil molecules and 1 rubber molecule, corresponding to a mass ratio of 80 wt% bio-oil to 20 wt% rubber. The molecular models of bio-oil, rubber, bio-oil-activated rubber, and BRR are shown in Figure 1. The BRR model was constructed using the Amorphous Cell module with a

target density of 1.0 g/cm^3. The COMPASS force field was employed, and all other simulation parameters were set to the default values of the system.

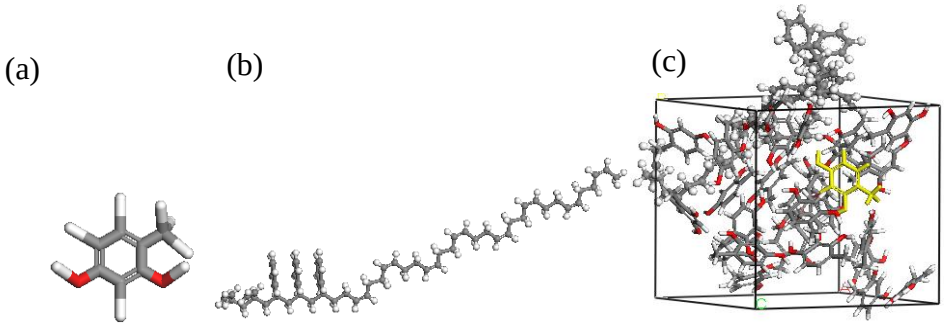

Figure 1. The molecular models of BRR system:(a)bio-oil, (b)rubber, (c)BRR

2.9 Molecular simulations

The molecular dynamic simulations were performed using Materials Studio 2024 software. The initial model was first geometrically optimized to get the stable configuration. In order to achieve the free volume fraction (FFV), radial distribution function (RDF), and Hansen Solubility Parameter (HSP), the NPT and NVT ensemble were used with a 100 ps molecular dynamic simulation. The time step selects 1 fs. The temperature and pressures are 298 k and 1 atm, respectively.

The free volume fraction (FFV) reflects the molecular mobility and permeability of the material. In this study, the Connolly surface method was used to calculate FFV.

The FFV calculation methods showed as equation (1).

$$FFV = \frac{V_f}{V} = \frac{V_f}{V_f + V_{oc}} \quad (1)$$

In the formula, V_f and V_{oc} respectively represent the free volume and occupied volume of the model.

The radial distribution function (RDF, g(r)) can be calculated for either one or two sets of atoms, which is related to the orderliness and arrangement of molecules

structure. The g(r) represents the change law of density function with distance from reference position, which is the probability parameter of the occurrence of a particular molecule at a distance from the reference point r. The RDF is calculated by Equation (2).

$$g(r) = \frac{1}{\rho 4\pi r^2 \Delta r} \frac{\sum_{j=1}^{N} \Delta N(r \to r + \Delta r)}{NT} \quad (2)$$

where ρ is the density of the system, r is the distance in the radial direction, Δr is the interval distance, ΔN is the interval number of atoms between the Δr distance, and N and T are the total number of atoms and total time of the system, respectively.

The Hansen Solubility Parameter (HSP) is a predictive framework for solubility based on intramolecular interaction principles. It quantifies molecular properties through three orthogonal dimensions: δ_D (dispersion forces), δ_P (polar forces), and δ_H (hydrogen bonding capacity). By decomposing substance-solvent interactions into these components, HSP enables systematic prediction of material compatibility and solubility behavior. The Hansen solubility parameter (δ) can be calculated by equation (3).

$$\delta^2 = (\delta_D)^2 + (\delta_P)^2 + (\delta_H)^2 \quad (3)$$

where δ_D, δ_p, and δ_H is the dispersion component, polar component, and hydrogen bond, respectively.

3. Results and discussions

3.1 Composition optimization of BRR

As shown in **Table 4**, analysis of the fundamental properties of bio-oil reveals that the wood/rubber ratio is the primary influencing factor, exerting a significant

impact on these properties, followed by co-liquefaction temperature, retention time, solvent, and finally catalyst. The density, 60 °C viscosity, aromatic content, and saturate content of the bio-oil all decrease with an increasing wood/rubber ratio, whereas the flash point increases under the same condition. Waste tire rubber is rich in high-molecular-weight aromatic compounds (e.g., styrene-butadiene) and carbon black, yielding viscous, dense, and highly aromatic bio-oil upon liquefaction. In contrast, wood-derived bio-oil consists mainly of lower- molecular-weight oxygenated compounds (e.g., phenols and alcohols) with fewer aromatic rings, leading to reduced density, viscosity, and aromatic content, and a higher flash point, when the wood/rubber ratio increases.

Similarly, as the co-liquefaction temperature rises, the density, 60°C viscosity, aromatic content, and saturate content decrease, while the flash point increases. Moderate temperature increase (e.g., from 180 °C to 200 °C) enhances cracking and dealkylation reactions, producing lighter molecules that reduce viscosity, density, and aromatics/saturates content, while volatilization of low-boiling compounds raises the flash point. However, excessive temperatures (>240 °C) risk secondary condensation, increasing viscosity. Thus, 200 °C represents an optimal balance.

The Al_2O_3 catalyst can selectively regulate the aromatic content in bio-oil, while the CeO_2 catalyst can selectively control the saturate content. These findings indicate that both the wood/rubber ratio and co-liquefaction temperature significantly affect the fundamental properties of bio-oil. Furthermore, Al_2O_3 and CeO_2 catalysts exhibit selective catalytic effects on specific components in bio-oil. The optimal preparation

parameters are determined as follows: a wood/rubber ratio of 6:4, a co-liquefaction temperature of 200 °C, water as the solvent, and the use of Al_2O_3 catalyst. Al_2O_3 promotes aromatization via its Lewis acid sites, selectively enhancing aromatic content, while CeO_2 favors saturation through redox-mediated hydrogenation. Given that moderate aromatics improve compatibility with aged asphalt, Al_2O_3 was selected as the optimal catalyst for high-performance bio-rubber rejuvenator production.

Table 4. The fundamental properties of bio-oil

Sample	15°C Density (g/cm^3)	60°C Viscosity (mPa.s)	Flash point (°C)	Aromatics (%)	Saturates (%)	Yield (%)
S1	1.15	64.5	325	24.2	26.4	19.1
S2	1.10	67.2	344	23.5	25.8	19.5
S3	1.08	69.5	365	23.1	25.1	20.1
S4	1.02	72.8	376	22.6	23.7	20.5
S5	0.98	75.5	392	22.1	23.5	19.2
S6	1.02	73.2	378	22.5	23.6	21.2
S7	1.01	74.5	379	22.3	23.3	22.7
S8	1.00	75.7	380	22.1	23.2	24.5
S9	0.99	76.9	382	21.8	23.1	27.3
S10	0.97	77.3	383	21.7	22.8	27.5
S11	1.02	72.9	377	22.6	23.7	22.0
S12	1.01	73.0	377	22.6	23.7	23.5
S13	1.00	73.2	378	22.5	23.6	25.2
S14	1.00	73.3	378	22.5	23.6	25.9
S15	1.00	73.4	379	22.5	23.5	26.2
S16	1.02	72.8	376	22.6	23.4	31.2
S17	1.02	72.9	376	22.6	23.4	26.5
S18	1.02	72.9	376	22.6	21.1	21.3
S19	1.02	73.0	377	21.5	23.3	21.8
S20	1.02	73.0	377	22.3	23.3	21.5

As shown in **Table 5**, an analysis of the fundamental properties of the BRR reveals the following: The viscosity (at 60 °C), flash point, and density (at 15 °C) of the BRR decrease with increasing bio-oil content, while both the saturates and aromatics content increase as the bio-oil content rises. Increasing bio-oil content

reduces viscosity, density, and flash point due to its low-molecular-weight oxygenates and volatile components, while simultaneously increasing saturates and aromatics-partly because lignin-derived phenolics are classified as aromatics and aliphatic oxygenates as saturates in standard compositional analysis.

With an increase in microwave power, the viscosity and flash point decrease, whereas the density, aromatics content, and saturates content remain virtually unchanged. Similarly, as microwave time increases, the viscosity and flash point exhibit a slight decrease, while the density, aromatics content, and saturates content show almost no variation. Within the studied range (2000 W, 60 s), microwave treatment primarily induces mild thermal effects-slightly reducing viscosity and flash point through heating and volatilization-without significantly altering chemical composition, indicating its role as a physical activation aid rather than a deep chemical modifier. The bio-oil content, not microwave parameters, is the key factor governing the rheological and compositional properties of the BRR.

Table 5. The fundamental properties of BRR

Number	15 °C Density (g/cm^3)	60 °C Viscosity (mPa.s)	Flash point (°C)	Aromatics (%)	Saturates (%)
S21	1.06	225	462	20.1	16.4
S22	1.05	213	438	20.3	16.7
S23	1.03	206	415	20.7	17.1
S24	1.00	186	386	21.2	17.6
S25	0.98	175	380	21.8	17.9
S26	1.00	182	381	21.3	17.8
S27	1.00	178	375	21.3	17.8
S28	1.00	183	383	21.3	17.8
S29	1.00	179	380	21.3	17.8
S30	1.00	176	377	21.3	17.8

The above results indicate that bio-oil content has a significant impact on the

fundamental properties of the BRR, whereas microwave power and microwave time exert almost no discernible effect on these properties. The optimal preparation parameters for the BRR are determined as follows: 30% bio-oil content, 2000 W microwave power, and 60 s microwave duration.

3.2 The chemical structure and composition analysis of BRR

3.2.1 The chemical structure analysis of BRR

As shown in **Figure 2(a)**, GC-MS analysis of the BRR reveals the presence of guaiacol, furfural, formic acid, levoglucosan, and styrene-butadiene rubber fragments. Formic acid imparts acidity to the BRR (pH ranging from 3 to 4), which may cause equipment corrosion. Guaiacol exhibits antioxidant properties and possesses a relatively high calorific value. Furfural influences the storage stability of the BRR, while levoglucosan is characterized by high oxygen content, high viscosity, and chemical instability. These results indicate that the BRR is acidic and highly oxygenated. Although its fundamental properties differ from those of base asphalt, it can effectively restore certain performance characteristics of aged asphalt, rendering it suitable as an asphalt rejuvenator.

As shown in **Figure 2(b)**, with increasing bio-oil content, the relative abundances of $C_{10}H_{18}$ and $C_{10}H_8$ show a decreasing trend, whereas those of $C_8H_{10}O$, C_6H_5OH (phenol) and C_7H_8O exhibit an increasing trend. Quantitative analysis shows that the $C_{10}H_{18}$ content ranges from 47.5% to 52.3%, $C_8H_{10}O$ from 11.2% to 17.3%, C_6H_5OH from 10.0% to 13.4%, C_6H_5OH from 8.5% to 9.3%, and $C_{10}H_8$ from 1.5% to 2.0%. This indicates that $C_{10}H_8$ is the dominant component in BRR, while $C_8H_{10}O$,

C_6H_5OH (phenol) and C_7H_8O are present at comparable levels, and $C_8H_{10}O$, C_6H_5OH (phenol) and C_7H_8O is the least abundant. Furthermore, different BRR formulations exhibit distinct chemical compositions, and bio-oil content significantly affects the overall chemical profile of BRR.

The microwave activation mechanism suggests that microwave irradiation cleaves the S-S and C-S cross-links in waste tire rubber, thereby enhancing molecular flexibility. The hydroxyl (-OH) and carbonyl (C=O) groups in bio-oil can subsequently react with the generated radical sites on the devulcanized rubber, forming a chemically integrated BRR.

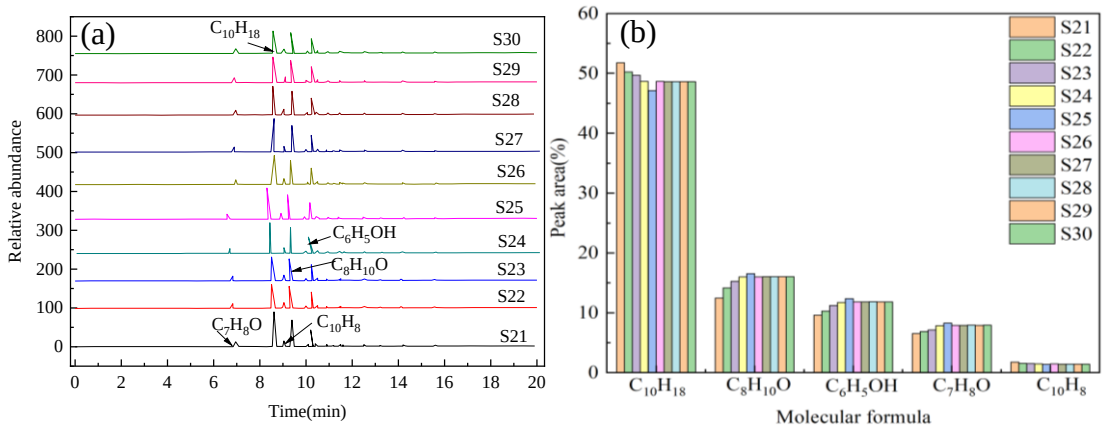

Figure 2. GC-MS of BRR: (a) GC-MS, (b) peak areas

3.2.2 The functional groups analysis of BRR

As shown in **Figure 3(a)**, the FT-IR spectrum of bio-oil exhibits characteristic absorption bands corresponding to O-H (hydroxyl), C=O (carbonyl), C-C, and C-H groups. The spectrum of waste tire rubber shows peaks associated with C-C, C-O-C (ether), C=O, C-S, C-H, N-H, and -N=C=O (isocyanate) functionalities.

The FT-IR spectrum of BRR is dominated by alkyl-related vibrational peaks, including 2925 cm^{-1} (asymmetric C-H stretching, possibly overlapping with O-H),

2860 cm^{-1} (symmetric C-H/C-C stretching), 1455 cm^{-1} (-CH_2- bending), 1378 cm^{-1} (-CH_3 bending), and 1170 cm^{-1} (C-O stretching). A distinctive aromatic ring vibration appears at 1600 cm^{-1}. The peaks at 2925 cm^{-1} and 2860 cm^{-1} are also characteristic of both cyclic and linear alkanes. The strong carbonyl (C=O) absorption at 1740 cm^{-1} in bio-oil is attributed to oleic acid or other fatty acid derivatives. Additionally, sulfoxide (S=O) groups give rise to a peak at 1030 cm^{-1}, while the C-S bond appears at 665 cm^{-1}.

These results indicate clear structural differences between bio-oil and BRR. During microwave-assisted preparation of bio-oil-activated rubber, chemical reactions occur, leading to cleavage of sulfur-containing cross-links (e.g., C-S and S-S bonds) and formation of new functional groups such as C=O and S=O. This process is referred to as microwave-induced devulcanization or desulfurization activation. Although the O–H group observed in BRR originates from bio-oil, its presence does not necessarily indicate a new chemical reaction. In contrast, when BRR is formulated by physically blending activated rubber with bio-oil, no further covalent chemical reactions take place; the resulting material is a composite rather than a chemically bonded product.

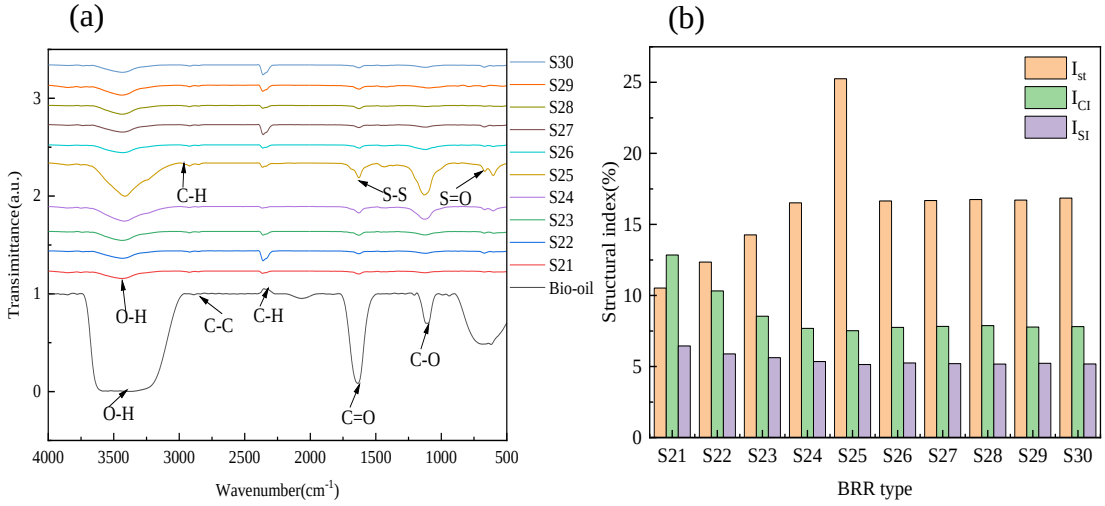

Figure 3. FT-IR and structural index of BRR: (a) FT-IR, (b) structural index

To quantitatively characterize the chemical structure difference in BRR, the characteristic peak area indexes of functional groups were evaluated. The characteristic functional groups indexes such as O-H, C=O, C-S, and S=O were pay attention because they can reflect the differences among the various components. The saturates index, carbonyl index (C=O), and sulphoxide index (S=O) were defined and calculated using peaks areas (A) according to equations (4) to (6).

Saturates index:

$$I_{st} = (A_{1235} + A_{1150}) / \sum A \tag{4}$$

Carbonyl index:

$$I_{CI} = A_{2358} / \sum A \tag{5}$$

Sulphoxide index:

$$I_{SI} = A_{1340} / \sum A \tag{6}$$

As shown in Figure 3(b), the saturates index, carbonyl index, and sulfoxide index of the BRR exhibit significant differences. The saturates index of BRR increases with higher bio-oil content, whereas both the sulfoxide index and carbonyl index decrease as bio-oil content rises. In contrast, with increasing microwave power and duration, the saturates index and carbonyl index of BRR increase, while the sulfoxide index decreases. These results indicate that bio-oil can promote the formation of saturates and carbonyl groups while inhibiting sulfoxide formation. Additionally, bio-oil can activate rubber. Overall, bio-oil content, microwave power, and microwave duration all exert an influence on the structural indexes and functional groups of BRR.

3.2.3 Molecular weight distributions analysis of BRR

The molecular weight distribution of different samples was calculated based on the following theoretical principles. Gel Permeation Chromatography (GPC) operates by separating molecules through porous gel fillers. In this process, larger molecules elute first, characterized by smaller elution volumes, while smaller molecules elute later, with larger elution volumes. By employing standard substances with known molecular weights, such as polystyrene, a calibration curve is constructed between the elution volume (Ve) and molecular weight (M). This calibration curve is typically represented in logarithmic form as: lgM = A-BVe. Subsequently, the GPC chromatogram of the BRR sample, which plots elution volume against signal intensity, is transformed into a molecular weight distribution curve, depicting molecular weight versus signal intensity, using the established calibration curve. This conversion allows for a quantitative analysis of the relative content of various molecular weight fractions.

The molecular weight distribution of BRR was characterized by gel permeation chromatography (GPC) to evaluate the influence of preparation parameters on its **macro-molecular** structure. As shown in **Figure 4**, larger molecules eluted at shorter retention times, consistent with the size-exclusion mechanism of GPC. The weight-average molecular weight (MW) of BRR exceeded 20,000 Da and increased with higher bio-oil content. Specifically, the peak molecular weight of neat bio-oil was approximately 20,010 Da, whereas that of BRR reached 21,300 Da, indicating that the incorporation of bio-oil into activated rubber resulted in a slight increase in

overall molecular weight compared to bio-oil alone. Notably, while the average molecular weight increased, the relative abundance of very high-molecular-weight species (>50,000 Da) decreased with increasing bio-oil content, suggesting a partial depolymerization or homogenization effect.

With increasing microwave power and irradiation duration, the molecular weight of BRR exhibited only a marginal increase, accompanied by a reduction in the refractive index detector (RID) signal−likely reflecting changes in sample concentration or compositional uniformity. Collectively, these results demonstrate that bio-oil content significantly influences the molecular weight distribution of BRR, whereas microwave power and treatment duration have negligible effects.

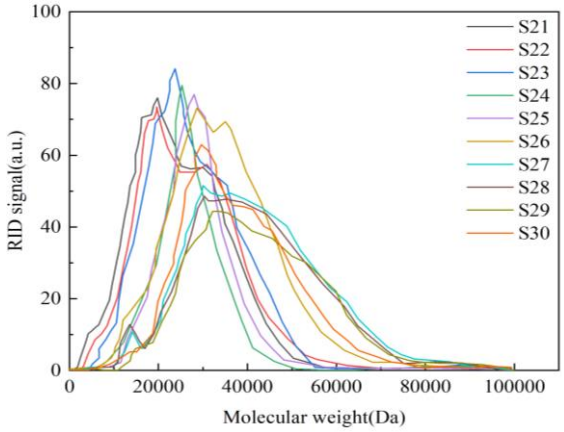

Figure 4. GPC of BRR

As shown in **Figure 5**, Fourier Transform Infrared Microscopy (FT-IRM) analysis of the BRR reveals significant differences in its FT-IR characteristics. The differences areas of FT-IR appeared at 2900-3000 cm^{-1} (C-H), 1680-1720 cm^{-1} (C=O), and 500-1200 cm^{-1} (fingerprint regions). Bio-oil, rich in oxygen-containing functional groups (e.g., C=O, -OH) and aliphatic chains, introduces distinct FT-IR signals when blended into rubber. The increased bio-oil content enhances C-H (2900-3000 cm^{-1})

and C=O (1680-1720 cm^{-1}) peaks and alters the fingerprint region (500-1200 cm^{-1}), reflecting its chemical contribution to the rejuvenator. Even within different regions of the same BRR sample, variations in the FT-IR curves are observed. With increasing bio-oil content, these differences in the FT-IR curves become increasingly pronounced. In contrast, increasing microwave power or duration results in almost no changes to the FT-IR curves of the BRR. These results indicate that bio-oil content significantly affects the FT-IR characteristics of the BRR, whereas microwave power and duration have only a minor influence on its FT-IR properties.

As shown in **Figure 5**, the FT-IRM analysis reveals characteristic peaks at 2930 cm^{-1} (C-H or O-H), 2862 cm^{-1} (C-C), 1740 cm^{-1} (C=O), 1457 cm^{-1} (-CH_2-), 1376 cm^{-1} (-CH_3-), 1168 cm^{-1} (C-O), and 1030 cm^{-1} (S=O). The BRR exhibits distinctive peaks at 2862 cm^{-1}, 1740 cm^{-1}, and 1030 cm^{-1}, which correspond to the presence of unsaturated hydrocarbon groups, sulfoxide groups, and oleic acid, respectively. The characteristic peak area associated with oleic acid increases with higher bio-oil content. These findings indicate that variations exist in the FT-IR characteristic peaks across different regions of the sample, confirming the occurrence of phase separation within the system. Notably, there are slight differences between the FT-IR and FT-IRM curves. This can be attributed to the fact that conventional FT-IR analyzes a single point, whereas FT-IRM examines an entire surface area.

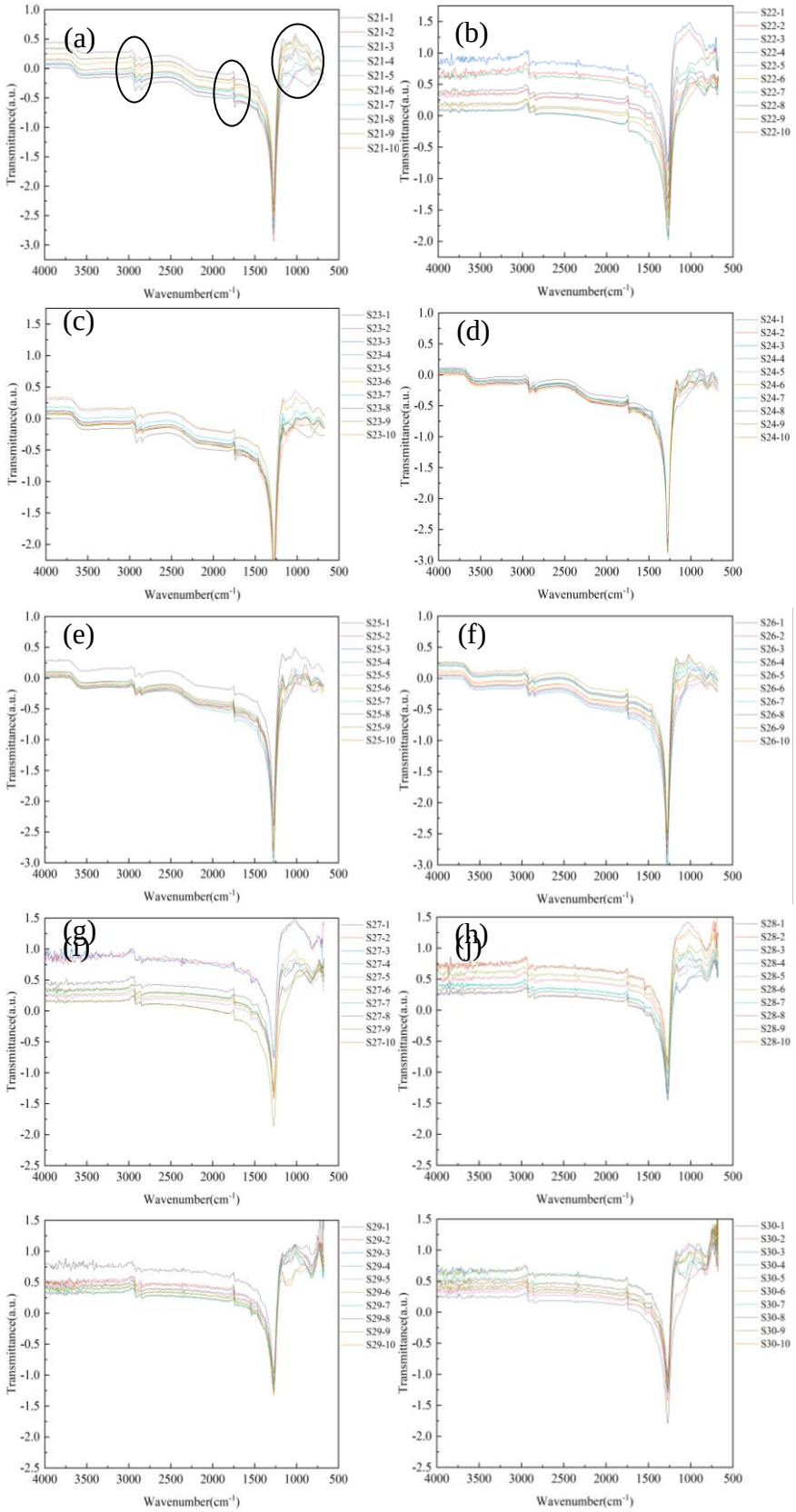

Figure 5. FT-IRM of BRR: (a)S21, (b)S22, (c)S23, (d)S24, (e)S25, (f)S26, (g)S27, (h)S28, (i)S29, (j)S30

3.2.4 The sulfur transformation of BRR

To elucidate the sulfur transformation mechanism, X-ray Photoelectron Spectroscopy (XPS) was employed to characterize the valence states of sulfur on the surface of the BRR. As illustrated in **Figure 6**, sulfur in the BRR (S21) existed in the forms of sulfate, sulfoxide, aliphatic sulfur, and sulfide. After the incorporation of bio-oil, the total content of sulfoxide and aliphatic sulfur in the BRR (S22) increased significantly, whereas the sulfide content decreased. Furthermore, in the BRR (S26), aliphatic sulfur was no longer detected, and thiophenic/elemental sulfur was generated instead—this phenomenon indicates that microwave power enhances the activation of rubber.

Based on the above results, the sulfur transformation mechanism during hydrothermal liquefaction is described by Equations (7) to (9). First, oxygen species (O*) in waste wood can oxidize sulfides into elemental sulfur. Subsequently, the elemental sulfur further reacts with carbon to form organic sulfur (C-S). When the microwave power is further increased to 1500 W, aliphatic sulfur is converted into thiophenic sulfur; this is attributed to the fact that high microwave power facilitates the occurrence of cyclization reactions.

$$S^{2-} + O^{*} \rightarrow S^{0} \quad (7)$$

$$S^{0} + C \rightarrow C - S \quad (8)$$

$$-CH_x - CH_y - S - CH_y - CH_{x-} \rightarrow C_4H_4S \quad (9)$$

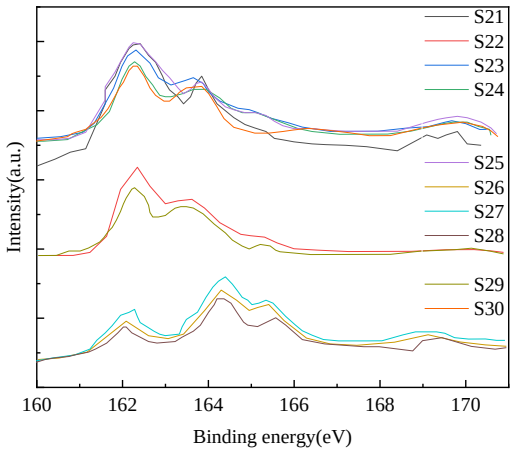

Figure 6. XPS of BRR

3.3 The rheological properties analysis of BRR

3.3.1 Viscosity-temperature curves analysis of BRR

As shown in **Figure 7**, the viscosity of BRR decreases monotonically with both increasing bio-oil content and temperature. The viscosity–temperature profiles exhibit strong non-linearity, characteristic of thermorheologically complex fluids. Among the tested formulations (S24, S26–S30), variations in microwave power and irradiation duration induce only minor shifts in these profiles. Collectively, these findings confirm that BRR displays significant temperature-dependent rheological behavior, with bio-oil content being the dominant factor governing its thermal sensitivity.

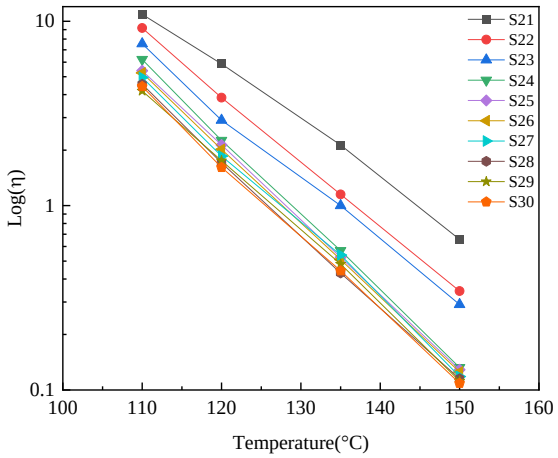

Figure 7. The viscosity-temperature curves of BRR

3.3.2 The high temperature rheological properties analysis of BRR

As illustrated in **Figure 8(a)**, the high-temperature rheological properties of BRR show that its complex modulus decreases with increasing test temperature and bio-oil content. The complex modulus also declines slightly with higher microwave power and longer irradiation duration; however, the influence of these microwave parameters is considerably weaker than that of temperature and bio-oil content.

This behavior stems from the fact that bio-oil content fundamentally alters the chemical composition, molecular structure, and overall properties of BRR, whereas microwave treatment primarily induces limited modifications to the rubber's functional groups or cross-link density. Consistent with this, the complex modulus exhibits only minor changes with increasing microwave power and duration. These results indicate that bio-oil significantly governs the high-temperature rheological response of BRR, while microwave parameters exert only a marginal effect. Overall, the bio-rubber rejuvenator behaves as a temperature-sensitive material, and its thermal sensitivity is strongly modulated by bio-oil content.

As shown in **Figure 8(b)**, the phase angle of BRR increases with rising test temperature and higher bio-oil content, and it also shows a slight upward trend with increased microwave power and irradiation time. These findings confirm that temperature and bio-oil content are the dominant factors influencing the phase angle, whereas microwave parameters play a secondary role. Notably, no abrupt transitions or discontinuities are observed in the phase angle curves, suggesting the absence of phase separation and good compatibility among the constituents of BRR.

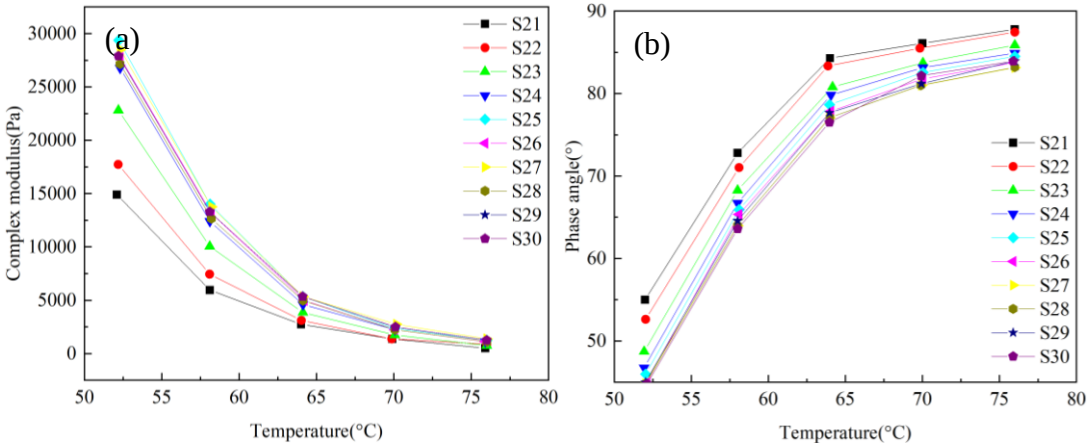

Figure 8. The temperature scanning curves of BRR: (a)complex modulus, (b)phase angle

3.3.3 The low temperature rheological properties analysis of BRR

As shown in **Figure 9**, the low-temperature cracking resistance of BRR increases with rising bio-oil content. Microwave power and irradiation duration also contribute to a modest improvement in this property. Collectively, these findings demonstrate that bio-oil is the primary factor governing the low-temperature rheological performance of BRR, effectively enhancing its anti-cracking capability, while microwave parameters exert only a secondary influence.

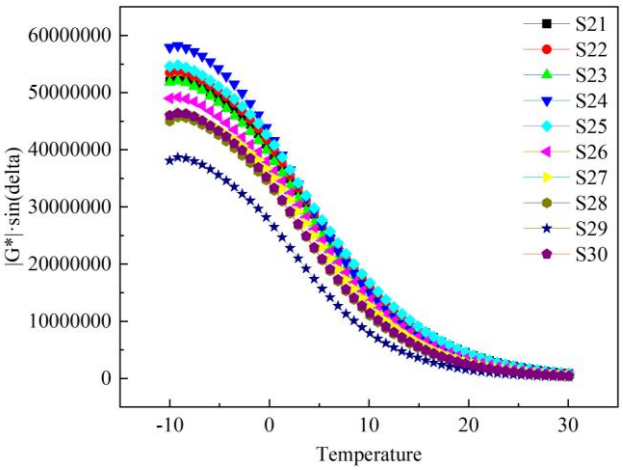

Figure 9. The low temperature anti-cracking factor of BRR

3.4 The microstructure analysis of BRR

3.4.1 The fluorescence microscopic morphology analysis of BRR

As shown in **Figure 10**, fluorescence microscopy revealed distinct morphological features in BRR: Blue-emitting regions correspond to fluorescent components, whereas dark areas represent non-fluorescent phases. The fluorescence intensity shows a strong positive correlation with bio-oil content (R^2 = 0.97), confirming that bio-oil contains intrinsic fluorescent moieties that enhance the overall luminescence. Although microwave treatment (1000–2000 W, 60–240 s) induced minor intensity variations (<8%), statistical analysis ($p > 0.05$) confirmed that microwave parameters have a negligible effect compared to bio-oil composition. These findings indicate that bio-oil content is the primary determinant of the fluorescence performance of BRR, governed by its native chromophores, while microwave processing offers a secondary means of fine-tuning the photoluminescent properties through combined control of bio-oil formulation and microwave exposure.

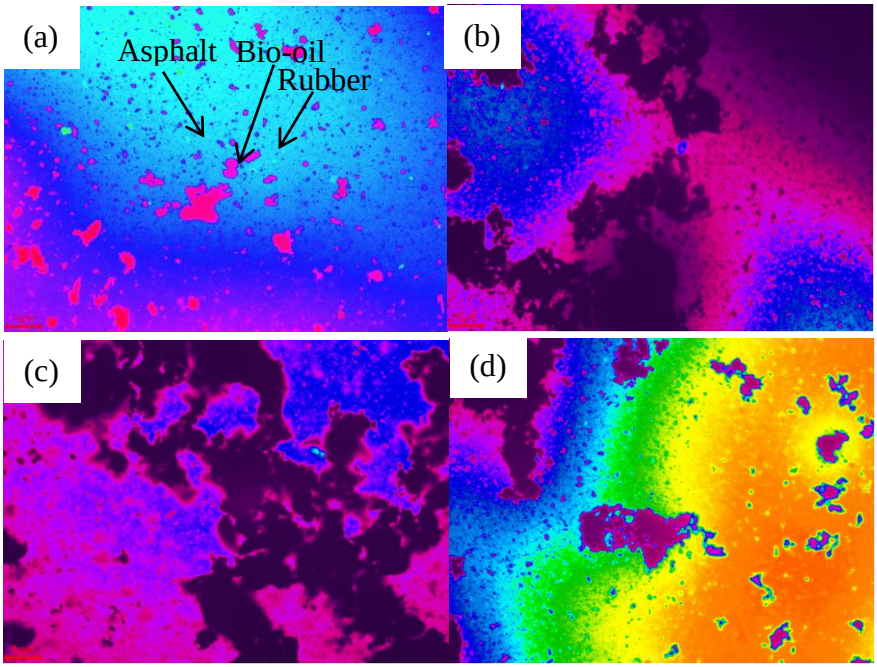

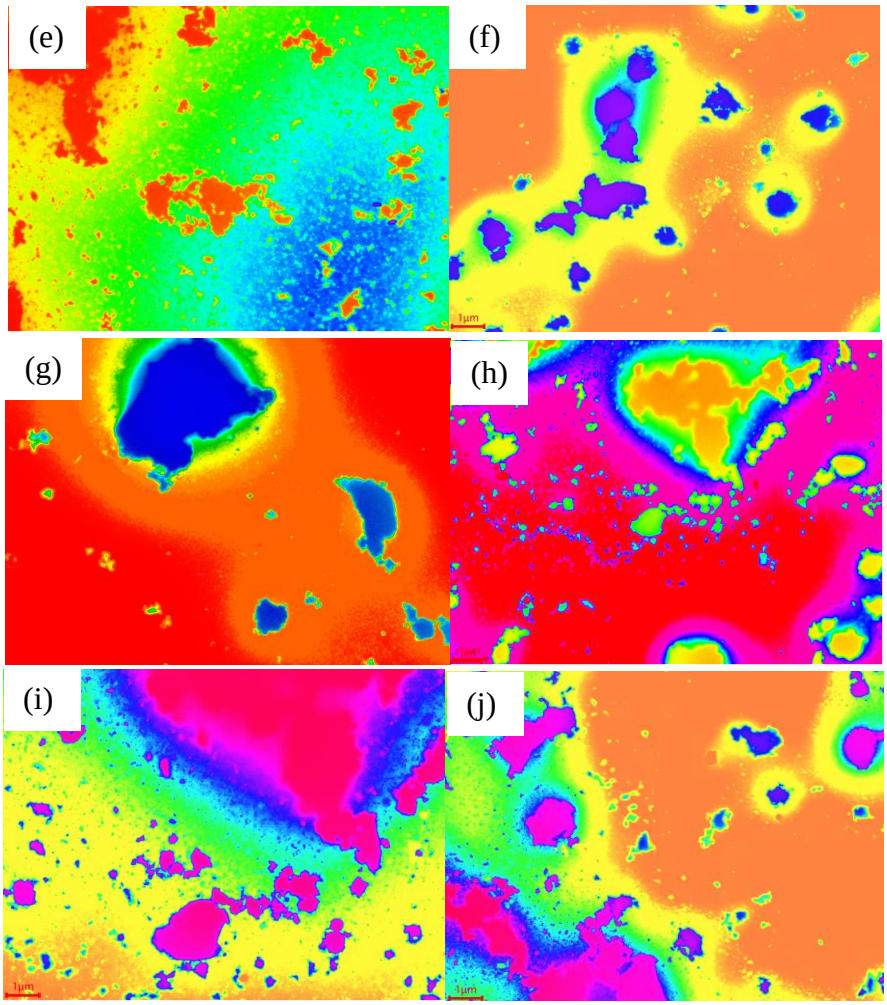

Figure 10. The fluorescence microscopic morphology of BRR: (a)S21, (b)S22, (c)S23, (d)S24, (e)S25, (f)S26, (g)S27, (h)S28, (i)S29, (j)S30

3.4.2 The free volume fraction analysis of BRR

As illustrated in **Figure 11**, the free volume fraction (FFV) of BRR exhibits distinct dependencies on composition and processing conditions: FFV increases monotonically with bio-oil content (15–35%), rising by approximately 1.2 percentage points for every 1% increase in bio-oil. In contrast, FFV decreases exponentially with increasing microwave power (1000–2000 W) and irradiation time (60–240 s) (R^2 = 0.96).

This positive correlation between FFV and molecular mobility is corroborated by

dynamic mechanical analysis, which shows that higher FFV values (>15%) are associated with a 40% reduction in the activation energy for segmental motion (E_a = 25 ± 3 kJ/mol at FFV = 18% versus E_a = 42 ± 5 kJ/mol at FFV = 12%).

These observations can be attributed to two competing mechanisms: (1) the incorporation of bio-oil introduces low-viscosity components (viscosity $\eta \approx 0.08$ Pa·s at 160 °C), which expand the amorphous domains and increase free volume; and (2) microwave irradiation induces cleavage of S–S cross-links (as confirmed by FT-IR) and chain scission, thereby reducing intermolecular spacing.

Collectively, these results demonstrate that while bio-oil enhances molecular mobility through plasticization, microwave treatment enables precise control over mobility via structural modification—allowing for tailored adjustment of BRR's rheological properties.

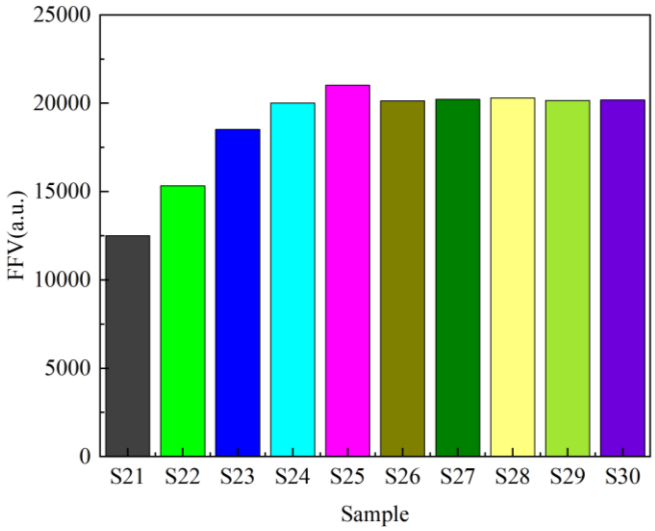

Figure 11. The FFV of BRR

3.4.3 The radial distribution function analysis of BRR

As illustrated in **Figure 12**, the radial distribution function (RDF) of BRR displays three characteristic peaks: the first corresponds to the nearest-neighbor

coordination shell, the second to the secondary shell, and the third to medium-range structural ordering. The overall RDF profile is sensitive to variations in bio-oil content, microwave power, and irradiation duration.

Specifically, the position of the first RDF peak shifts to higher inter-atomic distances with increasing bio-oil content, indicating disruption of short-range order. In contrast, this peak remains essentially unchanged with increasing microwave power and duration, suggesting that microwave treatment has negligible impact on the nearest-neighbor structure.

The second peak exhibits only minor variations under all tested conditions, implying that neither bio-oil incorporation nor microwave parameters significantly alter the intermediate-range local packing.

Meanwhile, the third peak becomes progressively broader and less pronounced as bio-oil content, microwave power, and irradiation time increase, reflecting a loss of medium- to long-range structural coherence. Collectively, these results demonstrate that bio-oil primarily governs the short-range disorder in BRR, while both bio-oil and microwave processing contribute to the degradation of longer-range structural order.

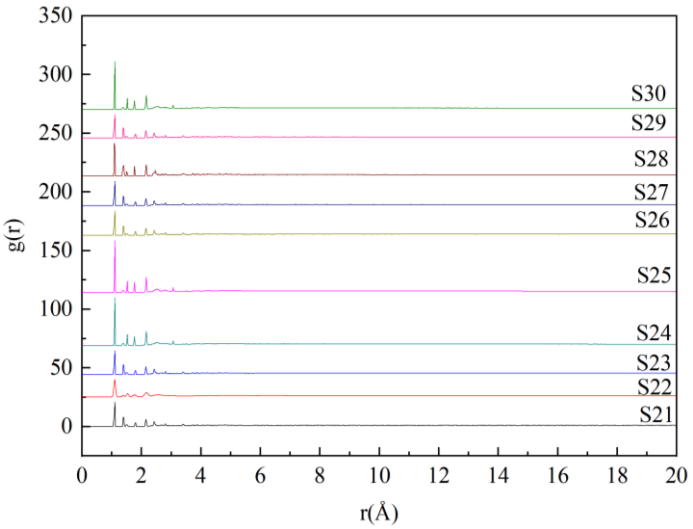

Figure 12. The RDF of BRR

3.4.4 The Hansen solubility parameter (HSP) analysis of BRR

As shown in **Figure 13**, Hansen solubility parameter (HSP) analysis reveals that the HSP of BRR is influenced by bio-oil content, microwave power, and irradiation duration. Specifically, increasing bio-oil content raises the total HSP (δ) of BRR and significantly reduces the HSP distance (*Ra*) relative to the base rubber, indicating improved compatibility between the bio-oil rejuvenator and the aged rubber matrix. In contrast, variations in microwave power and duration induce only marginal increases in δ and cause negligible changes in *Ra*. These findings suggest that while bio-oil plays a dominant role in enhancing interfacial compatibility, microwave treatment exerts minimal influence on the thermodynamic miscibility of BRR components.

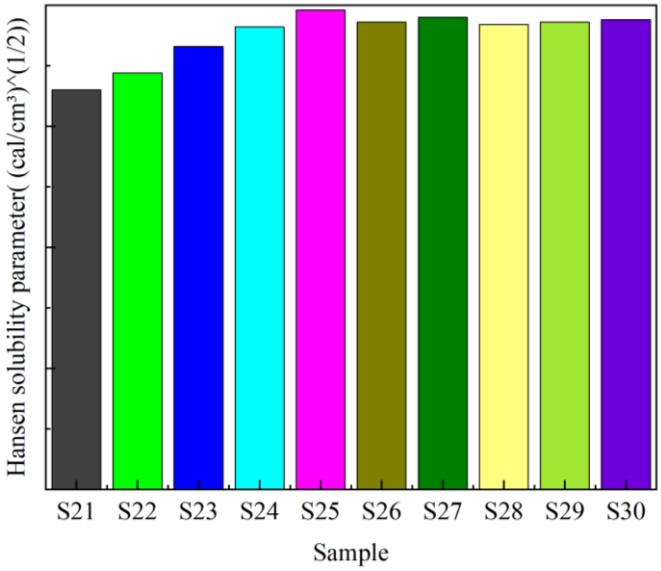

Figure 13. The Hansen solubility parameter (HSP) of BRR

3.5 The fundamental properties analysis of bio-rubber rejuvenator regenerated aged asphalt

As shown in **Table 6**, the fundamental properties of bio-rubber rejuvenator regenerated aged asphalt (BRRAA)—including penetration, softening point, and ductility—all satisfy the specification requirements for 70# asphalt. Specifically, increasing bio-oil content leads to a gradual increase in both penetration and ductility, while the softening point decreases correspondingly. This behavior stems from the plasticizing effect of bio-oil, which softens the aged asphalt matrix and improves its low-temperature deformability. Additionally, BRRAA exhibits a viscosity in the range of 1500-2500 mPa·s and an elastic recovery exceeding 60%, both of which comply with the performance criteria for regenerated asphalt binders.

In contrast, variations in microwave power and irradiation time induce only minor changes in these key indicators. These results indicate that bio-oil content is the dominant factor governing the fundamental properties of BRRAA, whereas

microwave parameters exert only a secondary influence. Overall, the BRRAA formulation meets all relevant specifications for high-quality regenerated asphalt.

Table 6. The fundamental properties of BRRAA

Material	Penetration (25 °C, 0.1 mm)	Softening point (°C)	Ductility (15 °C, cm)	Viscosity (135 °C, mPa·s)	Elastic recovery (25 °C, %)
70# asphalt	60-80	⩾46	⩾100	⩽3000	< 20
BRRAA-1	75	58	108	1501	69
BRRAA-2	71	55	125	1520	72
BRRAA-3	68	52	139	1600	75
BRRAA-4	63	49	145	1840	78
BRRAA-5	61	47	>150	1950	85
BRRAA-6	62	48	147	1890	81
BRRAA-7	61	46	149	2010	83
BRRAA-8	63	48	146	1860	80
BRRAA-9	62	48	147	1880	81
BRRAA-10	62	47	148	1900	82

3.6 The life cycle environmental impact assessment analysis of BRRAA

3.6.1 Goal and scope definition

This study conducted a comprehensive life cycle assessment (LCA) to evaluate the environmental performance of BRRAA. The primary objective was to provide evidence-based guidance for stakeholders considering BRRAA implementation in sustainable road construction. As illustrated in **Figure 14,** the system boundaries and functional unit were established following ISO 14040/44 standards.

The cradle-to-gate LCA framework encompassed four key stages: raw material acquisition and transportation (including biomass collection and waste tire recycling), BRR production and delivery, pavement construction (spreading and compaction), and end-of-life management (millings disposal or recycling). The functional unit was defined as 1km of BRRAA using regenerated 70# base asphalt. The optimal BRRAA

formulation, determined through prior experimental optimization (30% bio-oil content, 2000 W microwave treatment for 60 s), was applied in the regeneration of aged 70# asphalt to ensure representative environmental performance evaluation. Energy and Emission Calculation: Total energy consumption was determined by integrating the power demand of microwave heating, mixing, and auxiliary equipment over the processing time. Greenhouse gas emissions were derived by converting energy use into CO_2 equivalents using China's national grid emission factor, supplemented by upstream emissions from bio-oil and rubber powder production sourced from published LCA studies.

Figure 14. The boundaries conditions and functional unit of BRRAA

3.6.2 Life cycle inventory analysis

The inventory data collected for the LCA is categorized into primary and secondary data. Primary data is derived from calculations based on case studies in the relevant industry, representing the most up-to-date and accurate information. Secondary data is sourced from existing authoritative studies. The major indicators for

Life Cycle Impact Assessment (LCIA) include Global Warming Potential (GWP), Eutrophication Potential (EP), Photochemical Ozone Creation Potential (POCP), and Acidification Potential (AP). According to the conversion results of the life cycle inventory, the LCIA indicators for pollution emissions are presented in **Table 7**.

Table 7. Environmental impact categories and characterized factors

Impact category	Characteristic indicator	Pollution	Equivalent factor
GWP	CO_2	CO_2	1
		CH_4	25
		N_2O	298
EP	NO_3^-	NO_x	1.35
POCP	CH_4	CH_4	0.007
		CO_2	0.03
AP	SO_2	SO_2	1
		NO_x	0.7

Based on the statistical data presented above, the life-cycle energy consumption and gas emissions of BRRAA were calculated, with the results shown in **Table 8.** The trends for energy consumption, CO_2, N_2O, CO, SO_2, and NO_x emissions of BRRAA are consistent, following the order I>II>III>IV>V. However, the trends for CH_4 and CO_2 differ entirely, with CH_4 following the order I<II<II<IV<V.

Table 8. The energy consumption and gas emissions of BRRAA

Materials	Energy consumption (MJ)	CO_2 (kg)	CH_4 (kg)	N_2O (kg)	CO (kg)	SO_2 (kg)	NO_x (kg)
I	$1.95*10^7$	$1.89*10^5$	$2.28*10^1$	7.11	$1.25*10^3$	$1.45*10^3$	$3.05*10^2$
II	$1.89*10^6$	$1.59*10^5$	$3.15*10^1$	6.28	$8.38*10^2$	$8.48*10^2$	$2.48*10^2$
III	$1.65*10^6$	$1.42*10^5$	$3.26*10^1$	5.25	$6.25*10^2$	$6.35*10^2$	$2.05*10^2$
IV	$1,48*10^6$	$1.35*10^5$	$3.35*10^1$	4.32	$4.38*10^2$	$4.68*10^2$	$1.89*10^2$
V	$1.23*10^6$	$1.29*10^5$	$3.42*10^1$	3.58	$3.69*10^2$	$3.79*10^2$	$1.72*10^2$

Typically, CO_2 emissions are the highest (10^5 kg), dominating the overall gas emissions, while N_2O emissions are the lowest (10^0 kg), exerting the least impact. The

order of gas emission volumes is CO_2 >SO_2 >CO >NO_x >CH_4 >N_2O. This indicates that the energy consumption of BRRAA is lower than that of base asphalt; the trends for most gas emissions are similar, except for CH_4, whose emission trend is opposite. Furthermore, CO_2, SO_2, and CO dominate the gas emissions during the life-cycle assessment process, whereas CH_4 emissions have almost no impact on the overall gas emissions throughout the entire life-cycle assessment.

As shown in **Table 9**, the GWP trend of BRRAA is IV < III <V < II < I, while the EP trend of BRRAA is III < IV < V < II < I. Both POCP and AP of BRRAA exhibit the same trend: IV < V < III < II < I. The environmental indicators of BRR (I, II) are bigger than those of BRRAA (III, IV, V), indicating that BRRAA offer significant environmental advantages when used for high bio-oil content compared to conventional base asphalt. When considering only the emission equivalent mass, GWP is the most critical impact category in the LCA process. With the same binder (I and II), increasing the bio-oil content by 5% reduces GWP by 15%, indicating that the efficient utilization of bio-rubber rejuvenator can effectively mitigate global warming. However, the POCP and AP of BRRAA are reduced by an average of 20% and 25%, respectively, compared to base asphalt pavement, indicating a significant effect of BRRAA in reducing photochemical smog and Acidification.

Table 9. The LCA of BRRAA

Pavement type	GWP (kg)	EP (kg)	POCP (kg)	AP (kg)
I	$1.62*10^5$	$4.02*10^2$	$3.56*10^1$	$1.45*10^3$
II	$1.05*10^5$	$2.25*10^2$	$2.68*10^1$	$9.59*10^2$
III	$6.33*10^4$	$1.62*10^2$	$1.42*10^1$	$5.32*10^2$
IV	$6.19*10^4$	$2.12*10^2$	$7.89*10^0$	$2.26*10^2$
V	$6.38*10^4$	$2.18*10^2$	$7.92*10^0$	$2.31*10^2$

4. Conclusions

This study investigated the composition optimization and structure-property regulation of low-carbon **bio-rejuvenator** for aged asphalt. The key conclusions are as follows:

- The optimal preparation conditions for bio-oil are a waste wood-to-waste tire rubber ratio of 6:4, a co-liquefaction temperature of 200 °C, dichloromethane as the solvent, and Al_2O_3 as the catalyst. For the BRR, the optimal formulation comprises 30% bio-oil by weight, with microwave activation performed at 2000 W for 60 s.
- The BRR exhibits temperature-sensitive behavior, with its sensitivity strongly dependent on bio-oil content. Bio-oil significantly influences the rheological properties of the BRR, whereas microwave power and irradiation duration exert only minor effects.
- Bio-oil enhances molecular mobility within the BRR matrix. In contrast, excessive microwave power and prolonged irradiation may promote cross-linking, thereby restricting molecular motion. Furthermore, all three parameters, bio-oil content, microwave power, and irradiation time, affect the long-range structural disorder of the BRR.
- The BRRAA demonstrates lower energy consumption during production compared to conventional base asphalt. Moreover, the effective utilization of BRR contributes to reduced greenhouse gas emissions, offering potential environmental benefits in mitigating climate change.

Acknowledgments

This work was supported by the National Natural Science Foundation of China (No. 52378456), the National Natural Science Foundation of China International (Regional) Cooperation and Exchange Program (No. W2421062), the Shanxi Sanjin Youth Top Talent Project (SJYC2024308) and the Special Foundation of Achievements Transformation Guide of Department of Science and Technology of Shanxi Province (No.202204021301075).

References

[1] P. Bai. Z. Ma, L. Tian, Can government intervention correct and adjust resource misallocation of infrastructure: Evidence from toll expressway of China, Transportation Research Interdisciplinary Perspectives. 33 (2025) 101629.

[2] Z. Zhou, X. Yu, Y. Gao, W. Liu, Cost-effective optimization system for automated asphalt pavement maintenance, Automation in Construction. 177 (2025) 106333.

[3] K. Tsubasa, H. Kazuyoshi, Effect of privatizing Japanese expressway companies on maintenance and management efficiency, Transport Economics and Management. 3 (2025) 290-301.

[4] L. Zhang, R. Shi, J. Ning, L. Jia, K. Lee, RAMS assessment methodology for road transport self-contained energy systems considering source-load dual uncertainty, Renewable Energy. 239 (2025) 122096.

[5] S. Dong, Y. Tong, Z. Wan, C. Zuo, J. Luo, Z. Cui, H. Wang, Z. Dai, Multi-objective maintenance and rehabilitation decision-making modelling for highway networks: balancing economy, environment, and maintenance benefits,

Transportmetrica A Transport Science. 32 (2025) 2507898. DOI:10.1080/23249935.2025.2507898

[6] J. Ou, J. Zhang, H. Li, B. Duan, Road damage prediction and intelligent maintenance methods based on stacking ensemble learning, Advanced Engineering Informatics. 66 (2025) 103466.

[7] X. Yu, X. Lan, Z. Zhou, X. Nie, Effects of different dosages of iron ore tailings on the fatigue performance of high-strength modified AC asphalt mixtures, Construction and Building Materials. 494 (2025) 143367.

[8] Y. Sun, F. Zhang, D. Wang, W. Chen, F. Augusto, Study on the multiple recycling limit of asphalt binders containing high RAP content based on chemical and rheological properties, Fuel. 405 (2026) 136708.

[9] Y. Fan, H. Yu, Y. Zhou, R. Yang, J. Yang, W. Huang, Fracture characteristics and fracture surface recognition of epoxy-recycled mixtures with high reclaimed asphalt pavement (RAP) content toughened by SBS/CR-CSR, Theoretical and Applied Fracture Mechanics. 139 (2025) 105087.

[10] Y. Zhang, J. Li, T. Ma, H. Liu, C. Chen, J. Hao, Cold recycled mixtures prepared with finely separated RAP aggregates and modified emulsified asphalt: Adhesive performance and interface fusion characteristics, Construction and Building Materials. 493 (2025) 143122.

[11] S. Xu, G. Tang, S. Pan, Z. Ji, L. Fang, C. Zhang, Z. Cao, X. Zhou, X. Jia, Application of reactive rejuvenator in aged SBS modified asphalt regeneration: A review, Construction and Building Materials. 421 (2024) 135696.

[12] A. Gedik, Repurposing recycled walnut shell as an anti-aging agent into asphalt binder: A multi aspect evaluation, Construction and Building Materials. 498 (2025) 143969.

[13] N. Li, Y. Zhang, C. Bi, L. Xu, Experimental study on the horn effect of loaded patterned tires, Applied Acoustics. 242 (2026) 111053.

[14] M. Mahdi, K. Jozsef, Efficient flexible tire-terrain interaction modelling, Journal of Terramechanics. 120 (2025) 101081.

[15] X. Zhang, H. Wang, B. Thomas, Tire polishing effects on rubber-texture contact and friction characteristics of different asphalt mixtures, Wear. 582-583 (2025) 206328.

[16] D. Ren, J. Liang, Y. Cheng, L. Zheng, J. Chen, Z. Li, J. Li, Sustainable enhancement of rock asphalt composite binder using waste tire pyrolysis oil and rubber powder: a multi-scale study, Journal of Environmental Chemical Engineering. 25 (2025) 119356.

[17] S. Cui, R. Li, T. Yang, J. Wang, Z. Wang, X. Kai, Unveiling interactions of enzymatic hydrolysis lignin and waste tires during co-pyrolysis, Chemical Engineering Journal. 523 (2025) 168408.

[18] B. Meryem, C. Phuong, P. Warumporn, C. Benoit, G. Bertrand, N. Minh, C. Nedege, T. Joris, Performance comparison of tire pyrolysis oils in hydrotreating toward high-quality fuel, Chemical Engineering Journal. 520 (2025) 165115.

[19] X. Zhou, Z. Zhang, Metal organic frameworks catalytic co-pyrolysis mechanism of waste wood and rubber for oil preparation, Journal of the Energy Institute. 123

(2025) 102285.

[20] S. Alberto, N. Maria, V. Alberto, M. Juan, C. Maria, L. Jose, G. Tomas, M. Ramon, Pyrolysis of different types and sections of end-of-life tyres: Kinetics and experiments to improve product quality, Journal of Analytical and Applied Pyrolysis. 192 (2025) 107309.

[21] K. Wang, J. Zhan, H. Zang, X. Liu, H. Wang, Z. Peng, C. Wang, X. Tian, Study on in-situ and ex-situ catalytic pyrolysis of waste tires based on low-cost catalysts, Waste Management. 204 (2025) 114947.

[22] S. Towell, M. Ratushnyy, L. Cooke, G. Lewis, A. Zhukhovitskiy, Deconstruction of rubber via C–H amination and aza-Cope rearrangement, Nature. 640 (2025) 384-389.

[23] T. Mohamed, C. Antonio, O. López-Costas, P. Federico, Ł. Jeannette, Combining infrared spectroscopy (FTIR-ATR) and analytical pyrolysis for assessing chemical degradation pathways in waterlogged Neolithic wood, Journal of Analytical and Applied Pyrolysis. 191 (2025) 107197.

[24] D. Maximilian, H. Fabian, S. Ulrike, B. David, M. Marco, K. Thomas, Characterisation of beech wood pyrolysis oil: Chemical and physical properties and decomposition kinetics, Fuel. 404 (2025) 134897.

[25] L. Xu, Y. Chen, X. Song, Y. Qi, S. Li, H. Xu, Study on the pyrolysis process of engineered wood material with multicomponent modeling and peaks deconvolution analysis, Renewable Energy. 248 (2025) 123158.

[26] N. Li, K. Yan, R. Thanya, J. Liang, Y. Liu, Z. Wang, H. Nie, M. Suthawan, G.

Castiella-Ona, X. Pan, Q. Zhou, G. Jiang, G. Zhou, J. Ralph, J. Samec, F. Wang, Selective lignin arylation for biomass fractionation and benign bisphenols, Nature. 630 (2024) 381-386.

[27] S. Anna, H. Angela, P. Christoph, Exothermicity during the pyrolysis of large wood particles, Fuel Processing Technology. 27 (2025) 108250.

[28] S. Cheng, C. Tan, Y. Yu, J. Huang, J. Du, J. Hu, H. Wang, Targeted conversion of furfural from waste wood via catalyzed pyrolysis of acid-leaching residue, Bioresource Technology. 431 (2025) 132616.

[29] G. Cucci, F. Valentini, A. Dorigato, Cradle to gate life cycle assessment of Tyre-grade natural rubber produced in Thailand, Science of The Total Environment. 987 (2025) 179653.

[30] Y. Yang, T. Zhang, Y. Chen, C. Wang, G. Cai, A comprehensive review on application of scrap tire rubber for sustainable thermal insulation material in civil engineering, Renewable and Sustainable Energy Reviews. 217 (2025) 115727.

[31] J. Wang, C. Zhao, Q. Li, G. Song, Y. Hu, The synergistic effect of recycled steel fibers and rubber aggregates from waste tires on the basic properties, drying shrinkage, and pore structures of cement concrete, Construction and Building Materials. 470 (2025) 140574.

[32] Y. Wang, Y.Y. Wang, Experimental study and theoretical modeling of effective thermal conductivity of waste tire rubber composite concrete under different relative humidity, Journal of Building Engineering. 111 (2025) 113605.

[33] Q. Su, L. Xia, J. Tang, M. Zhang, D. Wang, D. Cao, From waste tires to long-life

asphalt pavement: Evaluation of rheological and fatigue properties of high-content rubber/SBS composite modified asphalt, Construction and Building Materials. 495 (2025) 143671.

[34] H. Wang, H. Yao, Y. Ma, S. Wang, X. Yu, S. Wang, Controllable decrosslinking of waste tire rubber as asphalt substitute: From elastic filler to colloidal rubberized asphalt, Fuel. 392 (2025) 134975.

[35] B. Zhang, G. Liang, B. Hou, Rubber running track inspired ultra-robust superhydrophobic coating armored with recycled tire rubber (RTR) particles for sustained corrosion resistance, Chemical Engineering Journal. 522 (2025) 167434.

[36] Z. Su, T. Zhou, S. Xie, C. Jin, L. Cao, Z. Dong, A. Gershome, M. Guo, Enhancing compatibility of crumb rubber in modified asphalt using green desulfurization for sustainable waste tire recycling, Construction and Building Materials. 490 (2025) 142556.

[37] N. Tian, T. Piergiorgio, Y. He, C. Sangiorgi, Surface treatment of waste tire rubber via oxidation and alkalization for enhanced compatibility with bitumen, Construction and Building Materials. 492 (2025) 142996.

[38] X. Jin, D. Ren, H. Wu, H. Kong, Q. Yang, T. Zhou, Z. Zhao, J. Li, Enhancing compatibility of waste tire rubber powder in asphalt: A comparative study of acid surface activation and molecular dynamics insights, Construction and Building Materials. 478 (2025) 141417.

[39] M. Zhang, Q. Su, G. Li, D. Cao, Y. Yao, S. Yang, S. Wang, Enhancing reutilization of waste tires and sustainability of environment: analysis of the

performance and emission reduction mechanism of high content rubber modified asphalt, Chemical Engineering Journal. 508 (2025) 160917.

[40] X. Zhou, M. Chen, S. Wu, X. Zhou, L. Li, Z. Ma, Heavy metals and PAHs adsorption characteristics of bio-asphalt in road runoff, Journal of Cleaner Production. 450 (2024) 141923.

Highlights

- Co-liquefaction of waste wood and waste tire rubber **was carried out to** produce bio-oil **in the presence of a catalyst.**
- **The bio-rejuvenator was synthesized by fine-tuning the bio-oil content and preparation parameters.**
- The microwave activation mechanism and **the regulation of** structure-property **relationships** of **the bio-rejuvenator** were elucidated.
- Oxygen species (O*) **present** in waste wood can oxidize sulfides **to** elemental sulfur.